

Machine Learning Enables Highly Accurate Predictions of Photophysical Properties of Organic Fluorescent Materials: Emission Wavelengths and Quantum Yields

Cheng-Wei Ju,^{*,†} Hanzhi Bai,[†] Bo Li,[†] and Rizhang Liu[†]



Cite This: *J. Chem. Inf. Model.* 2021, 61, 1053–1065



Read Online

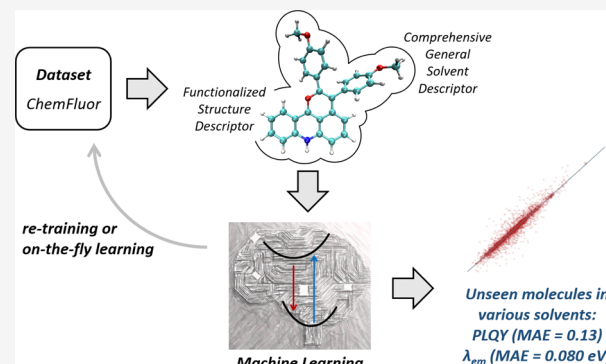
ACCESS |

Metrics & More

Article Recommendations

Supporting Information

ABSTRACT: The development of functional organic fluorescent materials calls for fast and accurate predictions of photophysical parameters for processes such as high-throughput virtual screening, while the task is challenged by the limitations of quantum mechanical calculations. We establish a database covering >4300 solvated organic fluorescent dyes with 3000 distinct compounds and develop a new machine learning approach aimed at efficient and accurate predictions of emission wavelength and photoluminescence quantum yield (PLQY). Our feature engineering has given rise to a functionalized structure descriptor (FSD) and a comprehensive general solvent descriptor (CGSD), whereby a highly black-box computational framework is realized with consistently good accuracy across different dye families, ability of describing substitution effects and solvent effects, efficiency for large-scale predictions, and workability with on-the-fly learning. Evaluations with unseen molecules suggest a remarkable mean absolute error of 0.13 for PLQY and 0.080 eV for emission energy, the latter comparable to time-dependent density functional theory (TD-DFT) calculations. An online prediction platform was constructed based on the ensemble model to make predictions in various solvents. Our statistical learning methodology will complement quantum mechanical calculations as an efficient alternative approach for the prediction of these parameters.



INTRODUCTION

Organic fluorescent materials, especially small-molecule organic fluorescent dyes, have been used extensively not only as useful tools in biological research^{1–4} but also as vital elements in material science.^{5–10} The last decades have seen the development of novel fluorescence-based applications including electrically pumped organic lasers,¹¹ stimulated emission depletion microscopy,^{12,13} thermally activated delayed fluorescence organic light-emitting diode,^{14,15} and so forth, attracting great attention to the rational design of organic materials with high photoluminescence quantum yields (PLQYs, Φ_{PL}) and precisely controlled maximum absorption and/or emission wavelengths (λ_{abs} , λ_{em}).^{16,17} Nevertheless, it remains a great challenge to predict Φ_{PL} with first-principles calculations.^{18–20} The high expense of excited-state calculations, combined with the involved interplay between radiative and non-radiative processes, has made it exceedingly costly to fully explore excited-state potential energy surfaces (PESs) without prior information.^{21,22} The situation is further compounded by the involvement of triplet excited states *via* intersystem crossing, whose modeling relies on accurate singlet–triplet gaps, spin–orbit coupling (SOC) strengths, and so forth.²³ For solvated organic dyes, the modeling of solvent, implicitly or explicitly, can lead to an array of

additional issues for solvent response, hydrogen bonding effects, and so forth, albeit dramatic dependence of Φ_{PL} on solvent is not any rare phenomenon.²⁴ As a neat quantum mechanical treatment, the thermal vibrational correlation function (TVCF) formalism developed by the Shuai group has been applied to the Φ_{PL} predictions of BODIPY²⁵ and rationalization of aggregation-induced emission (AIE)^{18,26} and room-temperature phosphorescence.^{27,28} However, successful TVCF calculations are still within a limited scope, and the efficiency is far from satisfactory for large-scale screening. Despite the efforts by Lin and Kohn *et al.* that develop semi-empirical methods to improve the efficiency (and accuracy) of Φ_{PL} predictions, the specific backbones and moderate accuracy [mean absolute errors (MAE) ≈ 0.2] again reflect the great challenge of Φ_{PL} predictions.^{23,29} Besides, the application of all these approaches requires details about the major photophysical processes. For the high-throughput screening of

Received: October 15, 2020

Published: February 23, 2021



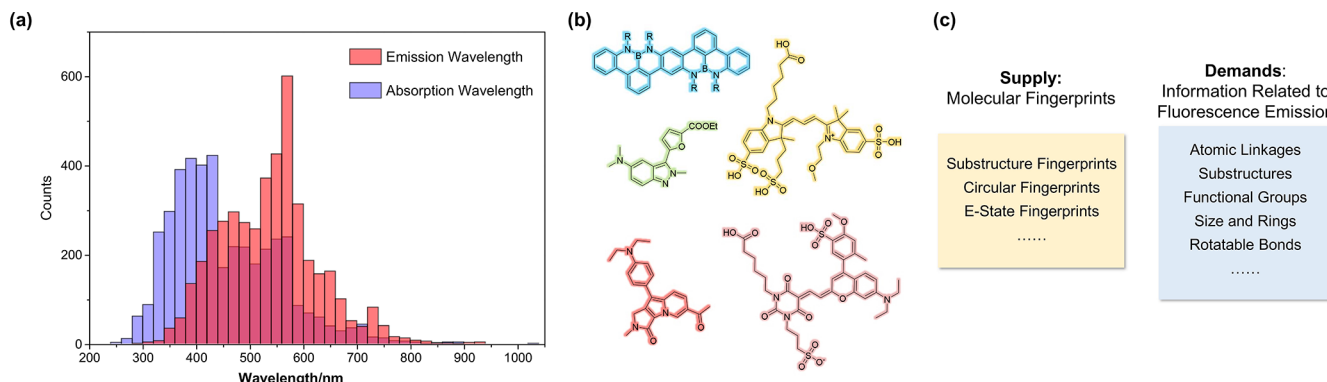


Figure 1. (a) Distribution of maximum absorption and emission wavelengths of the solvated organic fluorescent materials in our database. (b) Selective organic dyes in our database. (c) Illustration for the motivation of using multiple fingerprints.

organic materials with high Φ_{PL} , it is still strongly desired to develop a black-box computational framework with simple inputs, no requirement for pre-knowledge in photophysical processes, consistently good accuracy across different dye families, capability of describing substitution effects and necessary solvent effects, and efficiency for large-scale predictions.

Although the predictions of λ_{abs} and λ_{em} are much more tractable than Φ_{PL} , the commonly adopted computational methods, especially linear response time-dependent density functional theory (TD-DFT), are still in urgent need of improvement in various aspects.^{30–32} Seemingly a black-box method, the level of theory being used can have serious influences on the performance of TD-DFT.³³ In particular, the percentage of Hartree–Fock exchange greatly affects the description of charge-transfer excited states, the prediction of excited-state geometries (as in biaryl compounds), and, in many cases, the systematic overestimation of excitation/emission energies.^{34,35} Strategies such as optimal tuning can partly alleviate these issues but also creating a notable increase in computational expense that is inviable in the context of large-scale predictions.^{36,37} Moreover, TD-DFT is unavoidably biased toward certain backbones (e.g., even double hybrid functionals fail for cyanines).³⁸ Finally, the efficiency of TD-DFT calculations, especially taking its $O(N^4)$ scaling into account, can hardly meet the requirement for the large-scale screening of organic materials. Analogous to PLQY predictions, the fast, accurate, black-box prediction of λ_{abs} and λ_{em} with unbiased generality across different dyes is sought after in this work.

The difficulties in first-principles photophysical modelings have motivated us to explore a fundamentally different, top-down data-driven approach. In recent years, machine learning (ML) has exhibited enormous potential as a useful tool in medicinal chemistry,³⁹ organic synthesis,^{40,41} and material chemistry.^{42–44} For organic materials, although ML models have been established for various single-molecular properties available from (TD-)DFT calculations,^{45–47} predicting macroscopic characteristic parameters (activity, strength, durability, efficiency, etc.) based on molecular-level structural information is still a great challenge. So far, first principles can hardly predict these parameters. Reported ML predictions are limited to power conversion efficiency,^{48–52} gas absorption selectivity,^{53–55} and AIE effect,⁵⁶ most relying on expensive quantum mechanical calculations to generate input expressions. Most recently, the significance of basic photophysical parameters

have motivated the large-scale (nearly 12,000 molecules) machine-learning emission wavelength predictions.⁵⁷ However, for solvated molecules, the expression of solvent features is critical for improving overall accuracy but is rarely studied in detail.⁵⁸ To achieve large-scale predictions for emission wavelength and PLQYs with low/no sacrifice in accuracy, new strategies for feature engineering as well as the selection/designing of ML algorithms must be explored.

Herein, we report the development of highly accurate ML models for the fast estimation of photophysical parameters (λ_{abs} , λ_{em} , and Φ_{PL}) for solvated organic fluorescent materials. A database with more than 4300 experimental samples (around 3000 distinct compounds) and 11,000 data (λ_{abs} , λ_{em} , and Φ_{PL}) was established. A functionalized structure descriptor (FSD) and a comprehensive general solvent descriptor (CGSD) were developed and shown to be efficacious quantum-chemistry-free input expressions, enabling high-speed ML predictions. Remarkably, our optimal ML models predict Φ_{PL} with MAE = 0.11 and λ_{em} with MAE = 14.30 nm (0.066 eV in energy scale). This data-driven approach exhibits satisfactory universality toward unseen molecules and is systematically improvable *via* re-training and on-the-fly learning. Using our new solvent descript (CGSD), the pronounced change of PLQYs in different solvents can be predicted. A detailed comparison of our approach with TD-DFT calculations suggests dramatically less time cost for λ_{em} predictions (ML < 1 s vs TD-DFT ~50 CPU hours for each molecule) with a minor difference in accuracy. We made the ensemble model freely available at <http://www.chemfluor.top>, which will hopefully become a useful tool for the pre-screening and rational designing of organic fluorescent materials. Our work develops a new methodology for the prediction of organic fluorescent properties, and we believe that the scope of this method can be extended to more organic fluorescent materials. We believe that our black-box ML approach will serve as an efficient and reliable strategy that complements quantum mechanical calculations for the estimation of PYQYs as well as the high-speed prediction of emission wavelengths.

RESULTS

Importance of Descriptors and ML Algorithms for the Prediction of Emission and Absorption Wavelengths. Figure 1a shows the statistics of absorption/emission wavelengths (>4000 samples for around 3000 molecules, with >8000 wavelength data) collected from the literature. The data consist mainly of commercial fluorescent dyes and novel

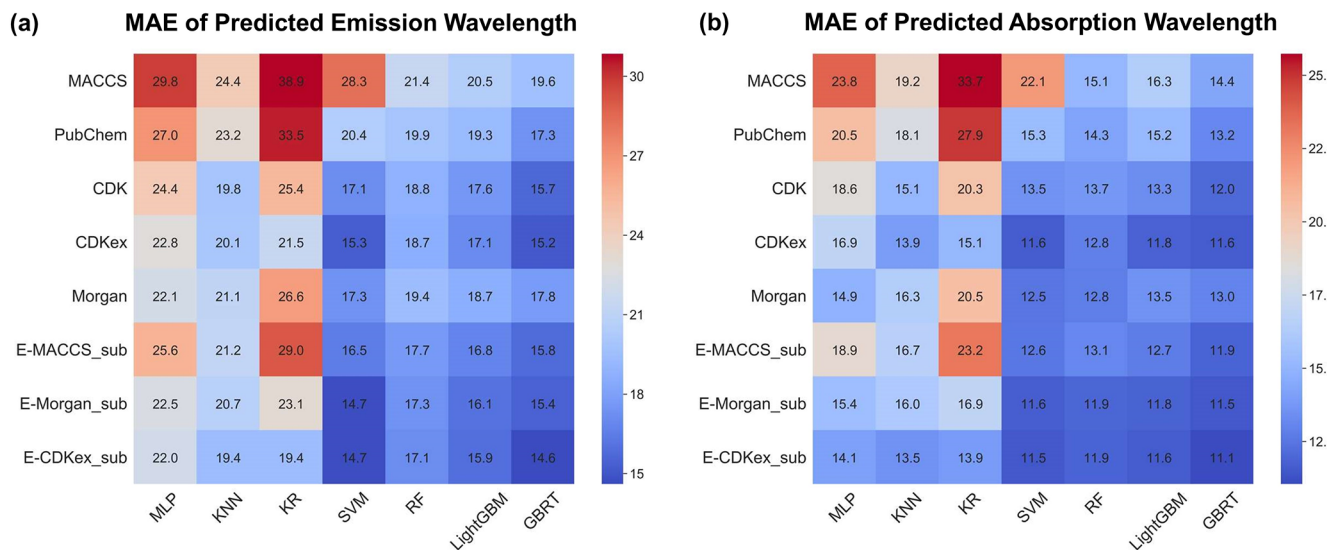


Figure 2. Testing results of (a) emission wavelength and (b) absorption wavelength of different combinations of ML models with different structure-based descriptors as inputs. The average MAE of 10 tests are shown in the center of each colored block; for each test, we randomly select 10% of the data as the test set and use the rest as the training set. Other metrics [R^2 , root mean squared error (RMSE) and their confidence intervals] can be found in Table S1 (Supporting Information). Details about the abbreviation of the FSD and fingerprints can be found in the Methods section in the Supporting Information.

organic molecules with fluorescent activity reported in recent years (Figure 1b), including various skeletons with different functional groups. Most of the emission wavelengths are distributed in the range of 400–700 nm (blue to near-infrared). One reason is that fluorescent dyes with longer emission wavelengths are believed to be conducive to the applications in biological imaging and have been synthesized extensively in recent years. Although another dataset has been reported recently, we believe that the scope of our own dataset is more suitable for the presenting study because most of the collected data, measured in the past 15 years, are considered more reliable and accurate in general, comprising a beneficial feature for ML.

In order to develop ML models, we started by the choice of molecular and solvent descriptors. Molecular descriptors serve as the basis for ML for it transforms molecular information into computer-readable data. Molecular fingerprints, a subclass of molecular descriptors available without any quantum mechanical calculation, are used in our study due to the high potential in high-throughput screening of materials. A potential challenge originates from the multifold molecular features involved in fluorescence emission, but a single molecular fingerprint hardly covers all of them (Figure 1c). For this reason, several kinds of fingerprints such as substructure key-based fingerprints and circular fingerprints as well as a handful of consensus fingerprints are investigated and compared. Furthermore, it is believed that the combination of fingerprints describing (a) molecular skeletons (circular fingerprints) and (b) functional groups is able to express the key structural features relevant to molecular photophysics. The presence (with small position dependence) of -Br, for example, can enhance SOC and thus facilitate intersystem crossing, a critical factor influencing PLQYs. As another example, rotatable bonds, which are closely related to non-radiative transitions, can be reflected by circular and substructure fingerprints. Moreover, although fingerprints cannot describe three-dimensional details such as conformations, the underlying structural roots could be reflected especially when fingerprints are

combined together. For instance, the molecular-structural basis for a biaryl compound to form a certain conformation ensemble lies mainly in the occurrence of a rotatable bond, the nature of the aryl skeletons, and functional groups, all of which could be captured if we use a set of combined fingerprints. We argue that the strategy of combining fingerprints will more efficiently enhance the expression of molecular structures.

Besides, because fluorescence properties are also sensitive to solvents especially for molecules with intramolecular charge transfer (ICT) features, CGSD, which combines $E_T(30)$ ⁵⁹ with other four empirical scales,⁶⁰ is proposed here in order to discern a wide spectrum of solvents.

The choice of the ML algorithm is key to precise prediction. In addition to random forest (RF),⁶¹ the most widely used ML algorithm, we also compared the performance and efficiency of other models including support vector machine (SVM),⁶² kernel ridge regression (KRR),⁶³ multi-layer perceptron (MLP),⁶⁴ k-nearest neighbor (kNN), light gradient boosting machine (LightGBM),⁶⁵ and gradient boost regression tree (GBRT)⁶⁶ to assess the relative merits of these approaches.

To gain preliminary insights into the predictive powers of these ML models in conjunction with various molecular fingerprints, we first compared their MAE for predicted absorption and emission wavelengths (Figure 2). In terms of tendency, shorter inputs show better performance with tree-based algorithms (RF, LightGBM, and GBRT), while kernel-based algorithms (KRR and SVM) become comparable to tree-based ones with long input features. MLP and kNN only show average results in our model, possibly because molecular fingerprints are sparse high-dimensional vectors. LightGBM, SVM, and GBRT regressors exhibit the lowest MAEs and are used for assessing fingerprints before further differentiation.

With regard to the efficacy of molecule descriptors,⁶⁷ substructure key-based fingerprints [MACCS (166 bits), PubChem (881 bits)], which are based on the presence of certain substructures in a limited structure list, exhibit poor performance according to Figure 2. By comparison, circular

Table 1. Performance of Selected Algorithms^a

prediction object	algorithms	<i>r</i>	<i>R</i> ²	MAE/nm	RMSE/nm	MAE/eV	RMSE/eV
emission	SVM	0.959 ± 0.009	0.918 ± 0.018	14.419 ± 0.683	25.736 ± 2.531	0.067 ± 0.003	0.126 ± 0.012
	LightGBM	0.957 ± 0.008	0.916 ± 0.016	15.295 ± 0.839	26.192 ± 2.044	0.071 ± 0.005	0.126 ± 0.013
	GBRT	0.962 ± 0.007	0.925 ± 0.014	14.307 ± 1.118	24.768 ± 2.238	0.066 ± 0.005	0.119 ± 0.012
absorption	SVM	0.975 ± 0.005	0.951 ± 0.010	11.187 ± 0.984	22.217 ± 2.625	0.076 ± 0.006	0.157 ± 0.015
	LightGBM	0.973 ± 0.005	0.946 ± 0.009	11.614 ± 0.548	23.177 ± 1.845	0.077 ± 0.005	0.156 ± 0.019
	GBRT	0.977 ± 0.005	0.954 ± 0.010	10.471 ± 1.023	21.459 ± 2.565	0.070 ± 0.006	0.146 ± 0.019

^aThe presented results for each algorithm are achieved by 10-fold cross validation. The standard deviation is obtained by the difference of the prediction of each fold.

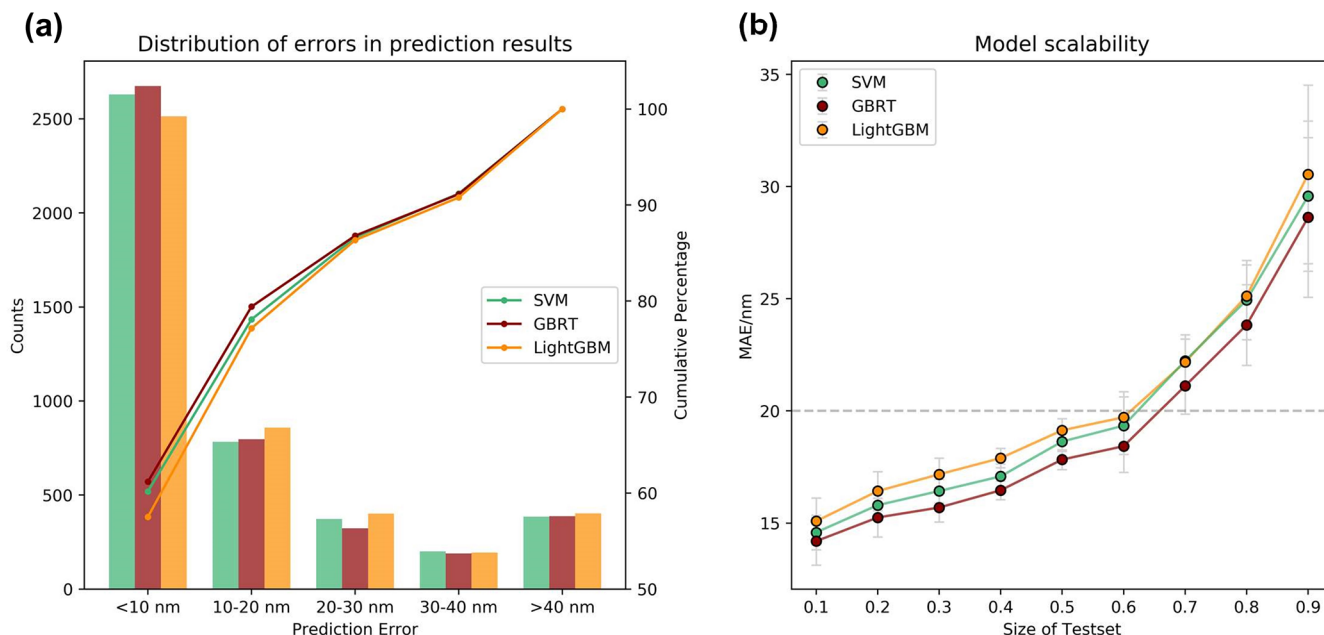


Figure 3. (a) Error distribution and (b) change of MAE with the increase of test set portion for SVM, GBRT, and LightGBM. FSD_CDK is employed in all these assessments.

fingerprints including chemistry development kit (CDK) fingerprints (1024 bits), CDK extended fingerprints (CDKex, 2048 bits), and Morgan fingerprints (2048 bits) show better performance, which implies that the representation of molecular structures by atom neighborhoods might be better for our purpose. In the recent study by Glorius *et al.*,⁶⁸ the benefits of combining multiple fingerprints features (MFFs) as a composite input molecular descriptor was demonstrated. However, due to the extreme lengths of MFFs (more than 70,000 bits), the resultant increase of computation cost limits its application. We propose that the combination of several descriptor describing features directly relevant to the phenomenon of interest might increase the efficiency of the expressions. Following this proposal, we have designed an FSD, which combines two circular fingerprints (CDKex and Morgan) with E-state fingerprints (79 bits) and substructure fingerprints [presence (307 bits) and count (307 number)], giving rise to FSD_CDK (E-CDKex_sub) and FSD_Morgan (E-Morgan_sub) (Figure 2). Both of these FSDs are sized 2741 bits. One key underlying motivation is that substructure fingerprints provide a differentiation for an array of functional groups, while structure descriptors (circular fingerprints) such as Morgan and CDKex are better expressions of the molecular backbones. Meeting our expectations, such a strategy does increase the performance for all algorithms considered here. We also applied this method to MACCS, the smallest

fingerprint, and the resulting E-MACCS_sub (length: 859 bits) also exhibits improved performance. These results indicate that composite inputs with multiple relevant features improve the performance of our ML models. The FSD_CDK gives the lowest MAEs in reproducing both emission and absorption wavelengths and are thereby used throughout the further assessments of ML algorithms. We attribute the success of FSD_CDX to the efficient incorporation of structural information that is most relevant to fluorescence emission.

To further differentiate SVM, LightGBM, and GBRT to find the optimal prediction model, we analyzed their performance with more metrics over our database with 10-fold cross-validation (Table 1; see Table S2 for other algorithms and Figures S2–S9 for scatter plots). Since in the TD-DFT studies, the MAE of eV is a more commonly used evaluation standard, we transformed the test result through the equation $E = 1240/\lambda$ to show the MAE of our models under eV. The superior performance of the GBRT regressor is consistently suggested by the lowest MAEs (10.47 nm and 0.70 eV for absorption, 14.31 nm and 0.66 eV for emission) as well as the highest coefficients of determination ($R^2 = 0.954$ for λ_{abs} and 0.925 for λ_{em}). In the prediction results of the absorption wavelength, the MAE is lower in the case of wavelength (nm) but higher in the case of energy (eV). This is completely acceptable and mainly due to the illusion brought about by the unit conversion. Due to the higher decision coefficients (R^2) and

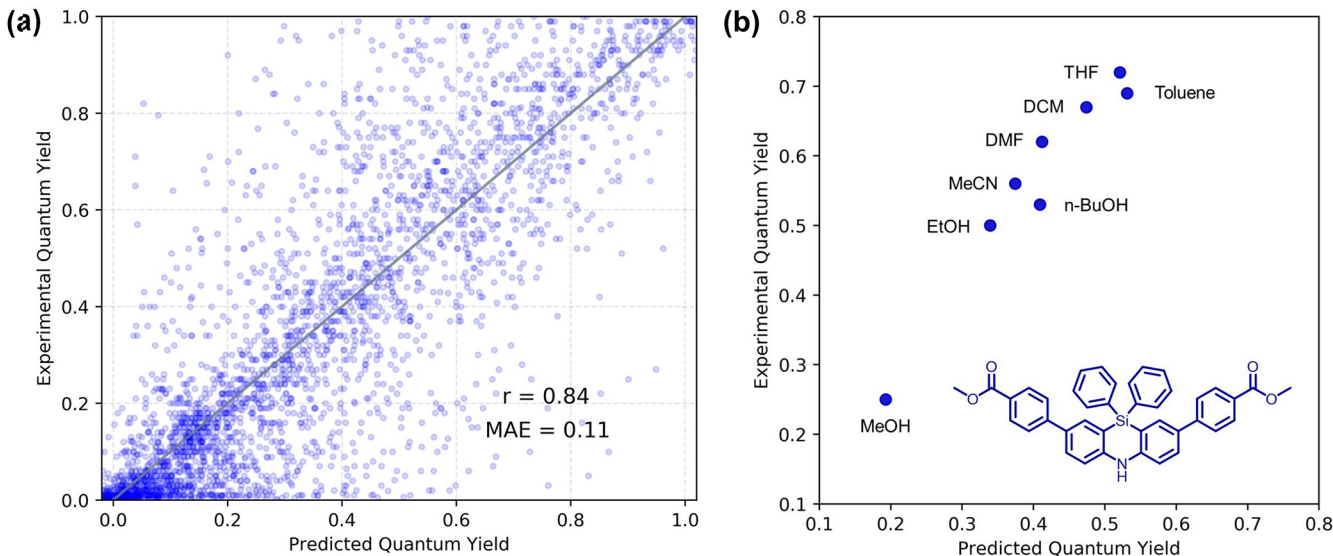


Figure 4. Prediction of PLQY with the ML regressor model. (a) Linear correlation between experimental PLQY and LightGBM-predicted values along with the correlation coefficient ($r = 0.84$). A perfect positive correlation is depicted by the solid diagonal line. (b) Chemical structures and quantum yield in different solvents of typical compounds which can be accurately predicted.

correlation coefficients (r), we argue that the ML models perform more reliably for absorptions. It is worth noting that although the prediction of absorption shows a higher accuracy (by R^2 and r ; plausibly due to the more direct structure–property relationship), more attention should be paid to emission due to the greater challenge of accurate prediction and the significance in fluorescence-based applications.

As described by Figure 3a (see Figure S1 for the rest of the algorithms), the advantage of GBRT over SVM and LightGBM is further supported by error distribution. The errors of more than 80% of the GBRT-predicted results are smaller than 20 nm, demonstrating the high accuracy of our approach for predicting molecules with similar backbones. Furthermore, it can be seen that GBRT has consistently larger cumulative percentage of error than the SVM and LightGBM. In order to further evaluate GBRT, SVM, and LightGBM by their upgradeability and universality, the dependence of MAE on the partition ratio of training/test sets was examined (Figure 3b). When the test set makes up increasingly higher portions, the MAE of all three regressors increases accordingly. Following this tendency, it can be inferred that our model can perform even better with more available training data, and the same conclusion has been suggested by the learning curve for the fixed dataset (Figures S11 and S12). The GBRT regressor, whose MAE remains smaller than 20 nm even when the training set is reduced to 40% of the entire database, shows smaller MAE than the other two models at all tested partition ratios. Therefore, with the analysis on performance metrics, error distribution, and model upgradeability, GBRT/FSD_CDK can be reasonably employed in further investigations to evaluate our ML approach.

We also investigated the feature importance for molecular structures. In accordance with our intuition, significant features in emission wavelength models include (a) total charge of molecules (7.6% for three parameters), an important character related to intramolecular charge transfer, (b) double bond counting (7.4%), which reflects skeleton conjugation, as well as (c) solvent descriptors (5.84% for CGSD). The importance of total charges is ascribed to the influences on ICT and

transition dipole moments, which are considered critical for fluorescent solvatochromism.

Due to the significance of solvent effects in organic photophysics,^{59,69} a successful model should be able to make predictions in the face of both new molecules and different solvents. Therefore, we have assessed our ML models for unlearnt organic dyes in different solvents to test the performance of CGSD. This is achieved by re-partitioning the database into training/test sets based on molecules, that is, the datapoints of the same molecules in different solvents will only appear in either training or test sets. In practice, we discriminate between molecules appearing only once (*part 1*) and molecules appearing multiple times in different solvents (*part 2*). Then, we randomly and separately chose 20% of the datapoints from *part 1* and *part 2* to form the test set. The performance of several algorithms following this approach is described in Table S3, which suggests that GBRT is the most suitable model for our purpose among the selected algorithms. The predictions by GBRT/FSD_CDK are shown in Figure S13. The overall MAE (17.36 nm, 0.0802 eV) is only slightly less accurate than randomly sampling 20% of the entire dataset (MAE: 15.25 nm, 0.0700 eV). Although *part 2* shows less satisfactory performance (MAE: 20.83 nm, 0.0933 eV for this part of the test set), such accuracy is still noticeable. To alleviate the error of *part 2*, we have devised and trained a stacking model using four ML models as base learners and the linear regressor as the meta learner (details and discussions can be found in the Supporting Information). This ensemble model has reduced the overall error to 17.20 nm, 0.800 eV and the *part 2* error to 19.79 nm, 0.0887 eV. The benefit of the ensemble model adds to the improvability of the ML approach. Nevertheless, we have continued to use a single GBRT model due to the following two reasons: (1) its high training efficiency (<5 min) promotes the potential on-the-fly learning, while the ensemble model needs a comparably much longer training time; (2) acceptable accuracy can be achieved by a single model since errors at the level of 1 nm/0.005 eV are not so obvious in practical applications.

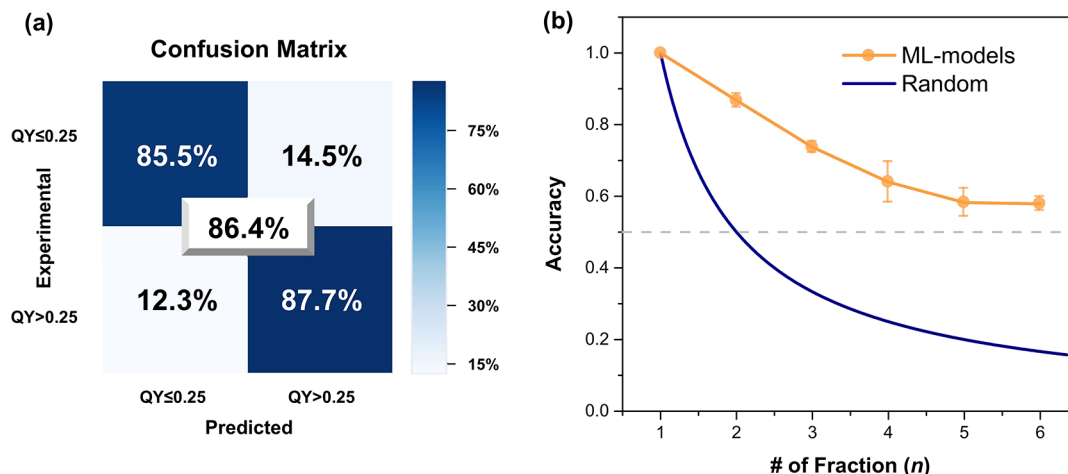


Figure 5. Prediction of PLQY with the ML classifier model. (a) Performance of the LightGBM classifier on the test set (10% datapoints randomly selected from the database). (b) Accuracy *versus* the number of fractions (*n*) obtained by the LightGBM model with FSD_CDK.

Summarizing this section, we have assessed an array of ML algorithms and molecular fingerprints for the prediction of absorption/emission wavelengths of solvated organic dyes, leading to the development of an ML regressor combining the GBRT algorithm, FSD_CDK, and CGSD. In the course of our evaluations, the GBRT algorithm shows optimal performance on our database according to multiple indicators, error analysis, and upgradeability comparisons. Regarding feature engineering, FSD_CDK has been developed by combining fingerprints describing features that are directly relevant to absorption and emission and have proven effective within the scope of our investigations. Furthermore, it has been demonstrated that our ML approach is improvable by the expansion of the database and the introduction of ensemble models. These results suggest the merits of our ML models for practical applications.

Exploration of Prediction of PLQY with ML Models.

PLQY is one of the most critical factors affecting the fluorescence intensity of organic fluorescent materials but attempts at its prediction are still limited. Oriented toward high-throughput screening of emissive organic materials, we hope to achieve the ML prediction of PLQY with efficient quantum-chemistry-free molecular representations. In our database, around 3000 PLQY data measured in various solvents have been collected. Screening over several fingerprints and algorithms indicate that the LightGBM/FSD_CDK regressor has optimal accuracy in our database (Tables S4 and S5). Reasonable accuracy is achieved with this regressor ($r = 0.84$, MAE = 0.11, $R^2 = 0.71$; see Figure 4a), which is sufficient for applications such as pre-screening of fluorophore candidates. In addition, if we only focused on the samples that are slightly bright (defined as $\Phi_{PL} > 0.10$ here), the MAE value is still 0.12, indicating the high performance of the ML model (Table S6). Moreover, the accuracy remains better than reported estimations with TD-DFT calculations²³ even when only 10% of our database is used for training (Figure S14 and Table S7), showing the superiority of our approach on this specific problem.

In attempts to reduce the error of our model, we noticed that experimental PLQY can have a large error bar. The best measurement method (integration sphere) may still have an error of about 10%, the relative method even higher. For this reason, we have investigated the effect of using only the high-quality data (~45% of the dataset) by absolute measurement.

As expected, the resultant accuracy ($r = 0.86$; see Figure S15 for details) is slightly improved even though the dataset is considerably smaller. According to this result, it is believed that our model can be further improved with more available high-quality PLQY data.

Analogous to absorption/emission wavelengths, we have also evaluated the impact of molecule-based partition on PLQY predictions to show the predictive power of our models in the face of solvent effects. The reasonably higher MAE (0.131) compared with the datapoint-based approach (0.120) suggests insignificant overfitting in our models. However, solvent effects have a more involved influence on PLQY than emission wavelengths—even the same molecule can display distinct PLQYs in different solvents. Questioning whether our models can discriminate between large solvent effects in the same compound, we have selected several organic dyes whose emission shows notable solvent dependence (Figures 4b and S18–S20). It is shown that the dramatic solvent effects have been well reproduced for these examples, which at least indicates the ability of our model for capturing the necessary solvent features for these molecules and suggesting the potential transferability to other cases. Further analysis suggests that our models can also differentiate the importance of the solvent for different photophysical parameters. The overall importance of CGSD follows the order of PLQY (LightGBM: 14.68%, GBRT: 11.84%) > emission (GBRT: 5.84%) > absorption (GBRT: 0.69%) (see Table S10 for details), which meets with our cognition on solvent effects.

We also investigated the importance of structural features contained in the FSD inputs. It agrees with our intuitions that the total charge of molecules (2.0%), count of aromatic rings (1.9%), presence of the 1,3-tautomerizable structure (1.5%), and number of rotatable bonds (1.1%) are identified as critical molecular-structural features for PLQY. The concurrent description of all these features by FSD is considered the basis for the high accuracy of our ML models. Although excited-state kinetics is not invoked in these models, we argue that molecular structures can be deterministic for the occurrence of certain excited-state processes. For instance, photoinduced structural planarization often relies on rotatable bonds in biaryl structures, and 1,3-tautomerizable structures have a close connection with reorganization energies. In addition, the charges are related to photoinduced electron

Table 2. Comparison between ML Models and TD-DFT Calculations for the Prediction of Emission Wavelengths^a

datasets	ML predictions ^b	TD-DFT calculations ^c			[refs]
		MAE/eV	MAE/eV	level of theory ^c	
large fluorescent dyes	skeletons	range of λ_{em}	0.121 ± 0.006 (for three classes of large fluorescent dyes)	0.350	TD-M06-2X/6-311+G(2d,p)/LR-PCM//TD-M06-2X/6-31G(d)/LR-PCM ³⁸
12 BODIPY-cyanines	600–850 nm				
11 D- π -A dyes	470–650 nm			0.100	TD- ω B97X-D/6-31+G(d,p)/LR-PCM//TD-CAM-B3LYP/6-31G(d)/LR-PCM ⁷⁵
11 rhodamine derivatives	530–600 nm			0.155	TD-B3LYP-D/6-31+G(d,p)/CPCM ⁷⁶
small fluorescent dyes	9 substituted benzoxadiazoles with 12 related molecules included into our dataset	370–500 nm	0.197 ± 0.016	0.308	TD-PBE0/6-31+G(d) ⁷⁷
49 coumarins with 8 coumarins randomly moved from test set to training set		350–500 nm	0.141 ± 0.020		
24 1,8-naphthalimides with 4 naphthalimides randomly moved from test set to training set		350–550 nm	0.234 ± 0.017	0.280	TD-PBE0/6-31+G(d)/LR-PCM ⁷⁸
overall	116 organic fluorescent materials (original training set)		0.142 ± 0.005		
	104 organic fluorescent materials (augmented training set)		0.220 ± 0.018	0.160	TD-PBE0/6-31+G(d)/LR-PCM ⁷⁹
			0.149 ± 0.010	0.237	
			0.149 ± 0.010	0.228	

^aSee Table S14 for details. ^bThe ML models are constructed with GBRT/FSD_CDk. ^cBest levels are chosen for each skeleton.

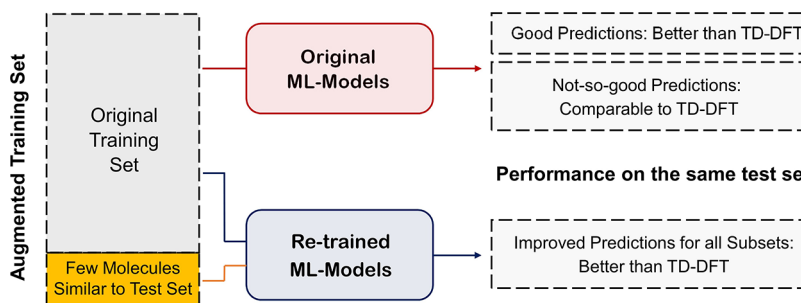


Figure 6. Schematic illustration for the improvement of ML models.

transfer as well as ICT characters, which have a significant influence on the brightness of organic materials. These input features, combined with the rest of the comprehensive structural information contained in FSD, comprise an ideal platform for a machine to directly learn the structural roots for PLQY, resulting in accurate ML models while avoiding the involved treatment of excited-state kinetics.

Seeking higher reliabilities than the regressors, we have also evaluated the performance of classifier models. To develop binary classifiers, the median of the experimental PLQY (0.25) was used as the threshold to equally divide the database into two groups. This threshold is also suitable in realistic applications. The performance of the LightGBM/FSD_CDK classifier is described by the confusion matrix in Figure 5a. The accuracies of the best-performing models for the first ($\Phi_{PL} < 0.25$) and second ($\Phi_{PL} > 0.25$) groups are 85.5 and 87.7%, respectively, giving rise to a satisfactory overall accuracy (86.8%). Further assessment suggests that the accuracy remains greater than 80% when the training set shrinks to only 40% of the dataset (Figure S21). Hence, functional organic materials with strong fluorescence ($\Phi_{PL} > 0.25$) can be identified by the ML binary classifier even when a relatively small training set is available.

With the binary classifier in hand, we hope to increase the resolution of our classifier by introducing multiclass classifier models. The dependence of accuracy on the number of groups (n) is given in Figure 5b. When $n = 3$, the overall accuracy remains at a reasonable level (73.7%; see Figure S22 for the confusion matrix). As n increases, the accuracy tends to decrease but is significantly superior to the random classifier. For $n = 6$, we can still obtain a 57.9% accuracy, which is around 3.5 times that of random classification. In fact, 68% of the incorrect predictions lie in intervals adjacent to the correct one (Figure S23), adding to the usability of our classifier. It can be inferred from the results here that ML classifier models are capable of providing reasonable predictions to PLQYs.

Because the binary classifier can already be applied to large-scale pre-screening of strong light-emission materials, we use it as example to test the accuracy of PLQY prediction on 22 molecules collected from three recent papers.^{70–72} Unfortunately, an average result was obtained (accuracy = 72.7%) (Figure S24 and Table S12). One of the underlying reasons might be the lack of negative data, that is, materials with weak/no fluorescence are often reported without quantum yields. But still, the recall of strong fluorescent materials can be achieved as 86.7%, which means that most tested molecules with strong fluorescence emission have been recognized by the binary classifier.

To conclude, we believe that our ML models, including regressors and classifiers, display reasonable accuracy in the

tests presented above. The expansion of the database is likely to enable further improvements that facilitate the design and virtual screening of novel organic fluorescent materials with high-quality ML predictions.

Comparison between ML Models and TD-DFT Calculations for Fluorescence Wavelength Predictions.

Whereas, in principle, quantum mechanical methods are efficacious as long as the physical approximations remain reasonable, empirical models such as QSAR and ML typically rely heavily on the scope of the training set and thereby lack universality. For example, the published QSAR studies on the relationship between molecular structures and photophysical properties are usually limited to a maximum of hundreds of molecules.^{73,74} It is therefore important to assess the scope of our ML model (hence the potential in real-world applications) for the prediction of emission wavelengths. Accordingly, we have collected 116 molecules from TD-DFT studies on vertical emission energies,^{38,75–79} mostly benchmark studies. The best levels of theories in each benchmark study were used to compare with our ML models. The ML-predicted emission wavelengths were translated into emission energies (eV) to be directly compared with TD-DFT. Note that the same level of error in wavelengths (nm) appears to be different when converted into energies (eV) due to the inverse proportionality ($E = 1240/\lambda$). To alleviate such effect, the set of 116 molecules are divided into two categories, namely, large fluorescent dyes whose emission wavelengths range from orange to red and smaller ones with blue-to-green fluorescence emissions.

The results of the assessment are summarized in Table 2. In terms of overall performance, our ML model displays a lower MAE than TD-DFT (0.200 eV for ML vs 0.237 eV for TD-DFT). The ML prediction of large fluorescent dyes seems excellent (MAE = 0.121 eV), superior to TD-DFT for BODIPY cyanines and rhodamine derivatives. In fact, these cyanines represent a particular challenge for TD-DFT calculations, which has been ascribed to the failure of TD-DFT for not correctly describing the difference of dynamic correlation between the two electronic states.³⁸ Even double-hybrid density functionals, which explicitly include contribution from virtual orbitals, give large errors for these molecules.⁸⁰ In contrast, our approach does not encounter such issue due to the direct statistical learning of experimental data, demonstrating the advantage of bypassing the physical framework. Although the MAEs of our models are generally larger for small fluorescent dyes, the performance is still comparable with TD-DFT for benzodiazoles (MAE = 0.197 eV) and coumarins (MAE = 0.234 eV) and is applicable to realistic problems. Since most small dyes collected in our dataset are novel heterocyclic dyes synthesized in the last decade and thus share fewer common features with this test

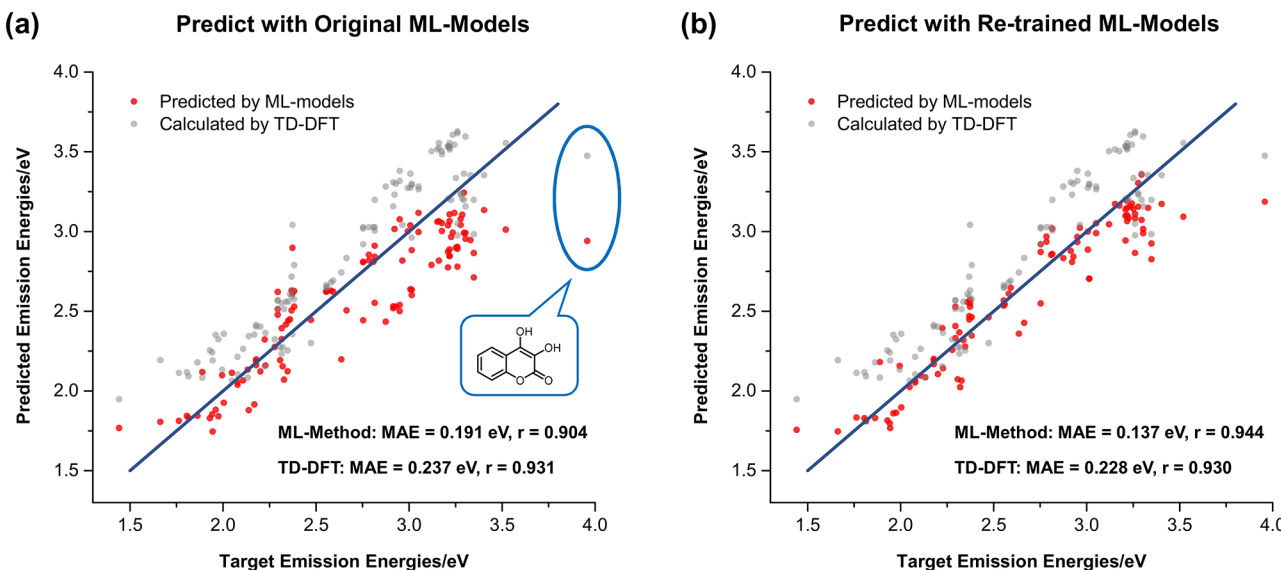


Figure 7. Fluorescence emission energies predicted by ML methods (red points) and modeled by vertical emission with TD-DFT (gray points). Results obtained with the original dataset (a) and the augmented database (b) are given. Perfect positive correlation ($r = 1$) is given by the blue lines for reference. The results of TD-DFT are slightly different from Table 2 because 12 molecules are moved from the test set to the training set.

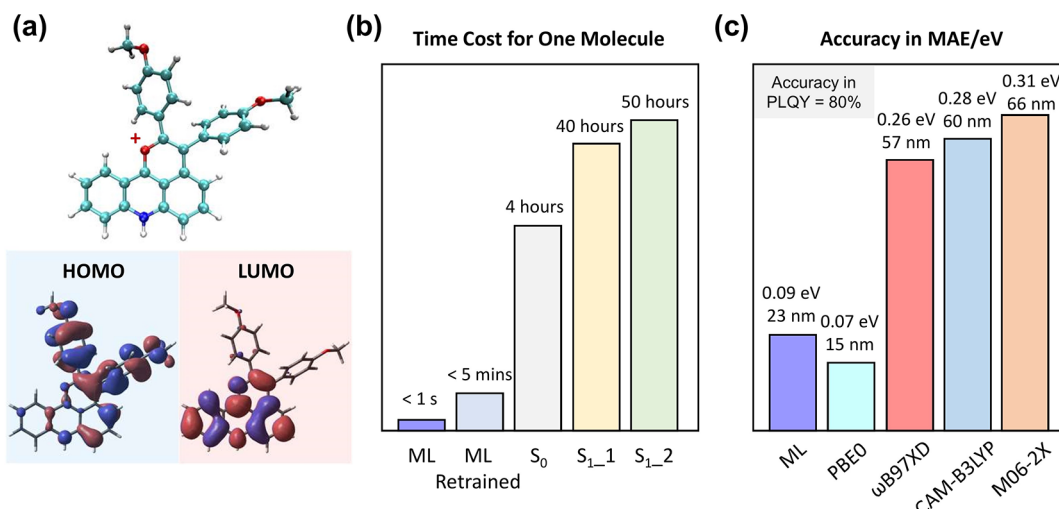


Figure 8. (a) Structure, HOMO, and LUMO of the representative molecule from the external dataset (30 molecules). (b) Comparison of the CPU time cost between the ML method and first-principles method (ES-2650v3). ML Retrained means the time cost with the re-trained process, which will not change with the increase of the molecule number. S_0 is only for optimizing the structure in the ground state; S_{1_1} means optimizing the excited structure in S1 with CAM-B3LYP/6-31G*/LR-PCM(DCM); S_{1_2} means after optimizing the excited structure in S_1 with CAM-B3LYP/6-31G*/LR-PCM(DCM), single points based on CAM-B3LYP/6-311+G*/LR-PCM(DCM) have been calculated. (c) Prediction accuracy of emission wavelength for this external dataset with the ML model and various functionals on 6-311+G*; prediction accuracy of PLQY is shown in gray color.

set, the relatively worse results on these molecules can be understood accordingly.

Although a prediction power comparable to TD-DFT is observed on the tested examples, there are still chances for the ML model to exhibit larger errors for more generalized cases. To demonstrate the applicability of our approach under such circumstances, we have investigated the improbability of our ML models for molecules with lower similarity to the training set, especially newly designed ones with unprecedented backbone structures. Note that aside from the original training set, learnable structural features might also be shared by certain subset(s) outside the training set (Figure 6). Inspired by this idea, we tested the impact of including a certain number of molecules analogous to the targeted ones into the training set.

Benzoxadiazole dyes were used for preliminary explorations because 12 characterized molecules with similar backbones were provided in the TD-DFT paper.⁷⁷ The effect of including the 12 datapoints was notable (MAE reduced to 0.141 eV), which meets with our expectation. For coumarins and naphthalimides, a different yet similar approach was investigated. We tried to move a small portion (<17%; randomly selected) of the test set into our training set. Again, the updated ML models show excellent performance (MAE = 0.142 and 0.149 eV, respectively). According to these results, we infer that the improvement of our ML models for less-learned backbones can be readily achieved by utilizing similar molecules as effective training data. The low cost of the (re-)training step (less than 5 min) is considerably lower than that

of TD-DFT computations. These results have also motivated us to provide a python script for both predictions and further expansion of database for learning on-the-fly, which is viable utilizing either more TD-DFT calculations or experimental feedback.

Figure 7a shows the correlation between experimentally measured emission energies and vertical emission energies calculated by TD-DFT and predicted by the ML model directly of the 116 molecules shown in Table 2. Compared with TD-DFT, ML shows a smaller MAE but worse correlation coefficient. The compound with the largest error is 3,4-dihydroxy-2H-chromen-2-one, for which the Lewis structure might deviate from the real one due to tautomerization. When the training set is augmented with a few molecules that are structurally related to the test set, the ML model exhibits better performance than TD-DFT computations (Figure 7b).

In order to further assess the performance of our ML methods, we collected 30 heterocyclic fluorescent dyes published recently as an additional test set.⁴ These dyes are ionic, a category that is missing from TD-DFT benchmark studies. Using experimental reference data, PLQYs are predicted with MAE = 0.21 for the ML regressor and 80% accuracy (*i.e.*, 24 out of 30 correct answers) for ML classifiers. These are considered good results given the difficulty of PLQY predictions. For emission wavelengths, we make use of this extra dataset to make another comparison between TD-DFT and our ML models. For part of the selected dyes, the FMO diagrams imply the charge-transfer character (Figure 8a). Our ML approach is able to make predictions costing less than 1 s for each molecule, reaching an overall MAE of 23 nm (0.09 eV). To contrast this with TD-DFT, we optimized all molecules in the S₁ state with TD-DFT at the level of CAM-B3LYP/6-31G*/LR-PCM(DCM) (a reference can be found in the Supporting Information). Then, emission energies were computed at the optimized geometries with 6-311+G*, a more extended Pople triple-zeta basis set equipped with polarization and diffuse functions for heavy atoms, in conjunction with the LR-PCM(DCM) solvent model and a series of typically recommended exchange–correlation functionals including hybrid functionals PBE0 and M06-2X as well as range-separated functionals ωB97X-D and CAM-B3LYP. These levels of theory are believed representative for realistic TD-DFT predictions. The accuracy and time cost with TD-DFT are compared with our ML models in Figure 8b,c (see Figure S26, Table S15, and Table S16 for details). It is suggested that PBE0 is the only functional showing lower MAE than ML on this dataset (15 nm, 0.07 eV for PBE0 vs 23 nm, 0.09 eV for ML). The MAEs with other functionals are in the range of 57–66 nm (0.26–0.31 eV), which are generally larger than those with ML models. Meanwhile, our ML approach shows a clear advantage in time cost since most TD-DFT predictions require 40–50 CPU hours.

From the comparison between TD-DFT and ML models, the following conclusions can be drawn: (1) by directly learning experimental data, ML models can predict a emission wavelength with a similar level of accuracy as TD-DFT in our tests, (2) improvement of ML models can be readily achieved by the introduction of a certain amount of data about organic dyes similar to the targeted one(s), implying potential for on-the-fly learning.

■ DISCUSSION

In summary, ML methodology was introduced to the predictions of photophysical parameters for organic fluorescent dyes. With a database of >4300 samples (~3000 solvated organic dyes in various solvents), ML models were developed. Molecular structures and solvent properties were efficiently expressed by the newly designed FSD and CGSD, respectively, and the underlying design rules were demonstrated. Combined with algorithm selection, ML prediction was realized for PLQYs with a good differentiation power in the solvent's degrees of freedom. For emission wavelengths, a thorough comparison between our ML approach and TD-DFT calculations was drawn, showing comparable accuracy and considerably lower time cost in the quantum-chemistry-free data-driven approach. Moreover, the improbability of our ML models was shown by the re-training process with additional datapoints. Our *ChemFluor* online ML prediction platform (<http://www.chemfluor.top>) will be a useful tool in the pre-screening by experimenters for discovery of new materials. Our work demonstrates how challenges in excited-state modeling especially those with highly involved physical nature (*e.g.*, quantum yields and potential lifetime, bandwidths, *etc.*) can be effectively solved by simple ML models. Meanwhile, we envision future improvements in the prediction accuracy, model generalizability, and transferability (*e.g.*, to non-organic materials) of data-driven predictions for materials properties as well as further explorations in material designing and discovery.

Despite our success in constructing ML models with good prediction power for emission wavelength and PLQY, we anticipate enhancement of interpretability by incorporation of first-principles philosophy.^{81–83} This can include direct data-driven prediction of rate constants (k_{p} , k_{ISC} , k_{nr} , ...) or, more fundamentally, excited-state PESs, spin–orbit coupling strengths, and so forth so that the detailed mechanism of excited state processes can be modeled with rate theories and time-resolved dynamics simulations. The interplay between data and theories is likely to inspire more and more computational models that push forward the boundary of predictivity and interpretability, whereby the development of new platforms for the discovery and rational design of new materials can be accelerated.

■ ASSOCIATED CONTENT

SI Supporting Information

The Supporting Information is available free of charge at <https://pubs.acs.org/doi/10.1021/acs.jcim.0c01203>.

Detailed information about the method, ensemble learning model, solvent effect, and model performance ([PDF](#))

■ AUTHOR INFORMATION

Corresponding Author

Cheng-Wei Ju – College of Chemistry, Nankai University, Tianjin 300071, China;  orcid.org/0000-0002-2250-8548; Email: nkuchemjcw@mail.nankai.edu.cn

Authors

Hanzhi Bai – Department of Electronic Engineering, Shanghai Jiao Tong University, Shanghai 200240, China
Bo Li – Department of Chemistry, School of Science, Tianjin University, Tianjin 300072, China

Rizhang Liu – College of Software Engineering, Sichuan University, Chengdu, Sichuan 610064, China

Complete contact information is available at:
<https://pubs.acs.org/10.1021/acs.jcim.0c01203>

Author Contributions

¹C.-W.J., H.B., B.L., and R.L. contributed equally.

Notes

The authors declare no competing financial interest.

The data and codes used in this study are available on our website (<http://www.chemfluor.top>) or databases.⁸⁴

ACKNOWLEDGMENTS

We are grateful to Yumiao Ma (BSJ Institute, Beijing) for providing computation facilities. We thank Dr. Zijie Qiu (Max Planck Institute for Polymer Research), Yu-Zhi Xu (South China University of Technology), Hao-Zhe Wang, Qian-Zhen Shao (both Nankai University), and Ziwei Fan for valuable discussions. We appreciate all researchers who reported the data collected in this study, especially Dr. Andreas Schüller (Pontificia Universidad Católica de Chile) and Prof. Dr. Young-Tae Chang (Pohang University of Science and Technology).

REFERENCES

- (1) Vendrell, M.; Zhai, D.; Er, J. C.; Chang, Y.-T. Combinatorial Strategies in Fluorescent Probe Development. *Chem. Rev.* **2012**, *112*, 4391–4420.
- (2) Lee, J.-S.; Kang, N.-y.; Kim, Y. K.; Samanta, A.; Feng, S.; Kim, H. K.; Vendrell, M.; Park, J. H.; Chang, Y.-T. Synthesis of a BODIPY Library and Its Application to the Development of Live Cell Glucagon Imaging Probe. *J. Am. Chem. Soc.* **2009**, *131*, 10077–10082.
- (3) Han, Q.; Lau, J. W.; Do, T. C.; Zhang, Z.; Xing, B. Near-Infrared Light Brightens Bacterial Disinfection: Recent Progress and Perspectives. *ACS Appl. Bio Mater.* **2020**, DOI: [10.1021/acsabm.0c01341](https://doi.org/10.1021/acsabm.0c01341).
- (4) Ma, W.; Zhang, L.; Shi, Y.; Ran, Y.; Liu, Y.; You, J. Molecular Engineering to Access Fluorescent Trackers of Organelles by Cyclization: Chemical Environment of Nitrogen Atom-Modulated Targets. *Adv. Funct. Mater.* **2020**, *30*, 2004511.
- (5) Kondo, Y.; Yoshiura, K.; Kitera, S.; Nishi, H.; Oda, S.; Gotoh, H.; Sasada, Y.; Yanai, M.; Hatakeyama, T. Narrowband deep-blue organic light-emitting diode featuring an organoboron-based emitter. *Nat. Photonics* **2019**, *13*, 678–682.
- (6) Chen, Q.; Zajaczkowski, W.; Seibel, J.; De Feyter, S.; Pisula, W.; Müllen, K.; Narita, A. Synthesis and helical supramolecular organization of discotic liquid crystalline dibenzo *h*₁*s*₁ ovalene. *J. Mater. Chem. C* **2019**, *7*, 12898–12906.
- (7) Qiu, Z.; Zhao, W.; Cao, M.; Wang, Y.; Lam, J. W. Y.; Zhang, Z.; Chen, X.; Tang, B. Z. Dynamic Visualization of Stress/Strain Distribution and Fatigue Crack Propagation by an Organic Mechanoresponsive AIE Luminogen. *Adv. Mater.* **2018**, *30*, 1803924.
- (8) Song, F.; Xu, Z.; Zhang, Q.; Zhao, Z.; Zhang, H.; Zhao, W.; Qiu, Z.; Qi, C.; Zhang, H.; Sung, H. H. Y.; Williams, I. D.; Lam, J. W. Y.; Zhao, Z.; Qin, A.; Ma, D.; Tang, B. Z. Highly Efficient Circularly Polarized Electroluminescence from Aggregation-Induced Emission Luminogens with Amplified Chirality and Delayed Fluorescence. *Adv. Funct. Mater.* **2018**, *28*, 1800051.
- (9) Coles, D. M.; Chen, Q.; Flatten, L. C.; Smith, J. M.; Müllen, K.; Narita, A.; Lidzey, D. G. Strong Exciton-Photon Coupling in a Nanographene Filled Microcavity. *Nano Lett.* **2017**, *17*, 5521–5525.
- (10) Yang, Z.; Mao, Z.; Xie, Z.; Zhang, Y.; Liu, S.; Zhao, J.; Xu, J.; Chi, Z.; Aldred, M. P. Recent advances in organic thermally activated delayed fluorescence materials. *Chem. Soc. Rev.* **2017**, *46*, 915–1016.
- (11) Liu, D.; De, J.; Gao, H.; Ma, S.; Ou, Q.; Li, S.; Qin, Z.; Dong, H.; Liao, Q.; Xu, B.; Peng, Q.; Shuai, Z.; Tian, W.; Fu, H.; Zhang, X.; Zhen, Y.; Hu, W. Organic Laser Molecule with High Mobility, High Photoluminescence Quantum Yield, and Deep-Blue Lasing Characteristics. *J. Am. Chem. Soc.* **2020**, *142*, 6332–6339.
- (12) Wang, C.; Fukazawa, A.; Taki, M.; Sato, Y.; Higashiyama, T.; Yamaguchi, S. A Phosphole Oxide Based Fluorescent Dye with Exceptional Resistance to Photobleaching: A Practical Tool for Continuous Imaging in STED Microscopy. *Angew. Chem., Int. Ed.* **2015**, *54*, 15213–15217.
- (13) Wang, C.; Taki, M.; Kajiwara, K.; Wang, J.; Yamaguchi, S. Phosphole-oxide-based Fluorescent Probe for Super-resolution Stimulated Emission Depletion (STED) Live Imaging of the Lysosome Membrane. *ACS Mater. Lett.* **2020**, *2*, 705–711.
- (14) Zhang, Q.; Li, B.; Huang, S.; Nomura, H.; Tanaka, H.; Adachi, C. Efficient blue organic light-emitting diodes employing thermally activated delayed fluorescence. *Nat. Photonics* **2014**, *8*, 326–332.
- (15) Lee, J.-H.; Chen, C.-H.; Lee, P.-H.; Lin, H.-Y.; Leung, M.-k.; Chiu, T.-L.; Lin, C.-F. Blue organic light-emitting diodes: current status, challenges, and future outlook. *J. Mater. Chem. C* **2019**, *7*, 5874–5888.
- (16) Kim, E.; Koh, M.; Lim, B. J.; Park, S. B. Emission wavelength prediction of a full-color-tunable fluorescent core skeleton, 9-aryl-1, 2-dihydronaphthalene [3, 4-b] indolizin-3-one. *J. Am. Chem. Soc.* **2011**, *133*, 6642–6649.
- (17) Carter, E. A. Challenges in modeling materials properties without experimental input. *Science* **2008**, *321*, 800–803.
- (18) Peng, Q.; Yi, Y.; Shuai, Z.; Shao, J. Toward quantitative prediction of molecular fluorescence quantum efficiency: Role of Duschinsky rotation. *J. Am. Chem. Soc.* **2007**, *129*, 9333–9339.
- (19) Shuai, Z.; Wang, D.; Peng, Q.; Geng, H. Computational Evaluation of Optoelectronic Properties for Organic/Carbon Materials. *Acc. Chem. Res.* **2014**, *47*, 3301–3309.
- (20) Humeniuk, A.; Bužančić, M.; Hoche, J.; Cerezo, J.; Mitrić, R.; Santoro, F.; Bonačić-Koutecký, V. Predicting fluorescence quantum yields for molecules in solution: A critical assessment of the harmonic approximation and the choice of the lineshape function. *J. Chem. Phys.* **2020**, *152*, 054107.
- (21) Polyak, I.; Hutton, L.; Crespo-Otero, R.; Barbatti, M.; Knowles, P. J. Ultrafast photoinduced dynamics of 1, 3-cyclohexadiene using XMS-CASPT2 surface hopping. *J. Chem. Theory Comput.* **2019**, *15*, 3929–3940.
- (22) Li, X.; Chung, L. W.; Morokuma, K. Photodynamics of all-trans retinal protonated schiff base in bacteriorhodopsin and methanol solution. *J. Chem. Theory Comput.* **2011**, *7*, 2694–2698.
- (23) Kohn, A. W.; Lin, Z.; Van Voorhis, T. Toward Prediction of Nonradiative Decay Pathways in Organic Compounds I: The Case of Naphthalene Quantum Yields. *J. Phys. Chem. C* **2019**, *123*, 15394–15402.
- (24) Chi, W.; Chen, J.; Liu, W.; Wang, C.; Qi, Q.; Qiao, Q.; Tan, T. M.; Xiong, K.; Liu, X.; Kang, K.; Chang, Y.-T.; Xu, Z.; Liu, X. A General Descriptor ΔE Enables the Quantitative Development of Luminescent Materials Based on Photoinduced Electron Transfer. *J. Am. Chem. Soc.* **2020**, *142*, 6777–6785.
- (25) Ou, Q.; Peng, Q.; Shuai, Z. Toward Quantitative Prediction of Fluorescence Quantum Efficiency by Combining Direct Vibrational Conversion and Surface Crossing: BODIPYs as an Example. *J. Phys. Chem. Lett.* **2020**, *11*, 7790–7797.
- (26) Zhao, W.; He, Z.; Lam, J. W. Y.; Peng, Q.; Ma, H.; Shuai, Z.; Bai, G.; Hao, J.; Tang, B. Z. Rational Molecular Design for Achieving Persistent and Efficient Pure Organic Room-Temperature Phosphorescence. *Chem* **2016**, *1*, 592–602.
- (27) Ma, H.; Yu, H.; Peng, Q.; An, Z.; Wang, D.; Shuai, Z. Hydrogen Bonding-Induced Morphology Dependence of Long-Lived Organic Room-Temperature Phosphorescence: A Computational Study. *J. Phys. Chem. Lett.* **2019**, *10*, 6948–6954.
- (28) Ma, H.; Peng, Q.; An, Z.; Huang, W.; Shuai, Z. Efficient and Long-Lived Room-Temperature Organic Phosphorescence: Theoretical Descriptors for Molecular Designs. *J. Am. Chem. Soc.* **2019**, *141*, 1010–1015.

- (29) Lin, Z.; Kohn, A. W.; Van Voorhis, T. Toward Prediction of Nonradiative Decay Pathways in Organic Compounds II: Two Internal Conversion Channels in BODIPYs. *J. Phys. Chem. C* **2020**, *124*, 3925–3938.
- (30) Loos, P.-F.; Scemama, A.; Blondel, A.; Garniron, Y.; Caffarel, M.; Jacquemin, D. A mountaineering strategy to excited states: Highly accurate reference energies and benchmarks. *J. Chem. Theory Comput.* **2018**, *14*, 4360–4379.
- (31) Grimme, S. A simplified Tamm-Dancoff density functional approach for the electronic excitation spectra of very large molecules. *J. Chem. Phys.* **2013**, *138*, 244104.
- (32) Seibert, J.; Bannwarth, C.; Grimme, S. Biomolecular structure information from high-speed quantum mechanical electronic spectra calculation. *J. Am. Chem. Soc.* **2017**, *139*, 11682–11685.
- (33) Laurent, A. D.; Jacquemin, D. TD-DFT benchmarks: a review. *Int. J. Quantum Chem.* **2013**, *113*, 2019–2039.
- (34) Jacquemin, D.; Mennucci, B.; Adamo, C. Excited-state calculations with TD-DFT: from benchmarks to simulations in complex environments. *Phys. Chem. Chem. Phys.* **2011**, *13*, 16987–16998.
- (35) Jacquemin, D.; Planchat, A.; Adamo, C.; Mennucci, B. TD-DFT assessment of functionals for optical 0–0 transitions in solvated dyes. *J. Chem. Theory Comput.* **2012**, *8*, 2359–2372.
- (36) Refaelly-Abramson, S.; Baer, R.; Kronik, L. Fundamental and excitation gaps in molecules of relevance for organic photovoltaics from an optimally tuned range-separated hybrid functional. *Phys. Rev. B: Condens. Matter Mater. Phys.* **2011**, *84*, 075144.
- (37) Rubesová, M.; Muchová, E.; Slavíček, P. Optimal Tuning of Range-Separated Hybrids for Solvated Molecules with Time-Dependent Density Functional Theory. *J. Chem. Theory Comput.* **2017**, *13*, 4972–4983.
- (38) Charaf-Eddin, A.; Le Guennic, B.; Jacquemin, D. Excited-states of BODIPY-cyanines: ultimate TD-DFT challenges? *RSC Adv.* **2014**, *4*, 49449–49456.
- (39) Subramanian, G.; Ramsundar, B.; Pande, V.; Denny, R. A. Computational Modeling of β -Secretase 1 (BACE-1) Inhibitors Using Ligand Based Approaches. *J. Chem. Inf. Model.* **2016**, *56*, 1936–1949.
- (40) Ahneman, D. T.; Estrada, J. G.; Lin, S.; Dreher, S. D.; Doyle, A. G. Predicting reaction performance in C–N cross-coupling using machine learning. *Science* **2018**, *360*, 186–190.
- (41) Granda, J. M.; Donina, L.; Dragone, V.; Long, D.-L.; Cronin, L. Controlling an organic synthesis robot with machine learning to search for new reactivity. *Nature* **2018**, *559*, 377–381.
- (42) Gu, G. H.; Noh, J.; Kim, I.; Jung, Y. Machine learning for renewable energy materials. *J. Mater. Chem. A* **2019**, *7*, 17096–17117.
- (43) Raccuglia, P.; Elbert, K. C.; Adler, P. D. F.; Falk, C.; Wenny, M. B.; Mollo, A.; Zeller, M.; Friedler, S. A.; Schrier, J.; Norquist, A. J. Machine-learning-assisted materials discovery using failed experiments. *Nature* **2016**, *533*, 73–76.
- (44) Butler, K. T.; Davies, D. W.; Cartwright, H.; Isayev, O.; Walsh, A. Machine learning for molecular and materials science. *Nature* **2018**, *559*, 547–555.
- (45) Gómez-Bombarelli, R.; Aguilera-Iparraguirre, J.; Hirzel, T. D.; Duvenaud, D.; Maclaurin, D.; Blood-Forsythe, M. A.; Chae, H. S.; Einzinger, M.; Ha, D.-G.; Wu, T.; Markopoulos, G.; Jeon, S.; Kang, H.; Miyazaki, H.; Numata, M.; Kim, S.; Huang, W.; Hong, S. I.; Baldo, M.; Adams, R. P.; Aspuru-Guzik, A. Design of efficient molecular organic light-emitting diodes by a high-throughput virtual screening and experimental approach. *Nat. Mater.* **2016**, *15*, 1120–1127.
- (46) Faber, F. A.; Hutchison, L.; Huang, B.; Gilmer, J.; Schoenholz, S. S.; Dahl, G. E.; Vinyals, O.; Kearnes, S.; Riley, P. F.; von Lilienfeld, O. A. Prediction Errors of Molecular Machine Learning Models Lower than Hybrid DFT Error. *J. Chem. Theory Comput.* **2017**, *13*, S255–S264.
- (47) Pereira, F.; Xiao, K.; Latino, D. A. R. S.; Wu, C.; Zhang, Q.; Aires-de-Sousa, J. Machine Learning Methods to Predict Density Functional Theory B3LYP Energies of HOMO and LUMO Orbitals. *J. Chem. Inf. Model.* **2017**, *57*, 11–21.
- (48) Nagasawa, S.; Al-Naamani, E.; Saeki, A. Computer-Aided Screening of Conjugated Polymers for Organic Solar Cell: Classification by Random Forest. *J. Phys. Chem. Lett.* **2018**, *9*, 2639–2646.
- (49) Sahu, H.; Rao, W.; Troisi, A.; Ma, H. Toward Predicting Efficiency of Organic Solar Cells via Machine Learning and Improved Descriptors. *Adv. Energy Mater.* **2018**, *8*, 1801032.
- (50) Lee, M. H. Insights from Machine Learning Techniques for Predicting the Efficiency of Fullerene Derivatives-Based Ternary Organic Solar Cells at Ternary Blend Design. *Adv. Energy Mater.* **2019**, *9*, 1900891.
- (51) Sahu, H.; Ma, H. Unraveling Correlations between Molecular Properties and Device Parameters of Organic Solar Cells Using Machine Learning. *J. Phys. Chem. Lett.* **2019**, *10*, 7277–7284.
- (52) Sun, W.; Zheng, Y.; Yang, K.; Zhang, Q.; Shah, A. A.; Wu, Z.; Sun, Y.; Feng, L.; Chen, D.; Xiao, Z.; Lu, S.; Li, Y.; Sun, K. Machine learning-assisted molecular design and efficiency prediction for high-performance organic photovoltaic materials. *Sci. Adv.* **2019**, *5*, No. eaay4275.
- (53) Ma, X.; Li, Z.; Achenie, L. E. K.; Xin, H. Machine-Learning-Augmented Chemisorption Model for CO₂ Electroreduction Catalyst Screening. *J. Phys. Chem. Lett.* **2015**, *6*, 3528–3533.
- (54) Wang, S.; Zhang, Z.; Dai, S.; Jiang, D.-e. Insights into CO₂/N₂ Selectivity in Porous Carbons from Deep Learning. *ACS Mater. Lett.* **2019**, *1*, 558–563.
- (55) Zhang, Z.; Schott, J. A.; Liu, M.; Chen, H.; Lu, X.; Sumpter, B. G.; Fu, J.; Dai, S. Prediction of Carbon Dioxide Adsorption via Deep Learning. *Angew. Chem. Int. Ed.* **2019**, *58*, 259–263.
- (56) Qiu, J.; Wang, K.; Lian, Z.; Yang, X.; Huang, W.; Qin, A.; Wang, Q.; Tian, J.; Tang, B.; Zhang, S. Prediction and understanding of AIE effect by quantum mechanics-aided machine-learning algorithm. *Chem. Commun.* **2018**, *54*, 7955–7958.
- (57) Ye, Z.-R.; Huang, I.-S.; Chan, Y.-T.; Li, Z.-J.; Liao, C.-C.; Tsai, H.-R.; Hsieh, M.-C.; Chang, C.-C.; Tsai, M.-K. Predicting the emission wavelength of organic molecules using a combinatorial QSAR and machine learning approach. *RSC Adv.* **2020**, *10*, 23834–23841.
- (58) Yang, Q.; Li, Y.; Yang, J. D.; Liu, Y.; Zhang, L.; Luo, S.; Cheng, J. P. Holistic Prediction of the pKa in Diverse Solvents Based on a Machine-Learning Approach. *Angew. Chem.* **2020**, *59*, 19282–19291.
- (59) Reichardt, C. Solvatochromic Dyes as Solvent Polarity Indicators. *Chem. Rev.* **1994**, *94*, 2319–2358.
- (60) Catalán, J. Toward a Generalized Treatment of the Solvent Effect Based on Four Empirical Scales: Dipolarity (SdP, a New Scale), Polarizability (SP), Acidity (SA), and Basicity (SB) of the Medium. *J. Phys. Chem. B* **2009**, *113*, 5951–5960.
- (61) Breiman, L. Random forests. *Mach. Learn.* **2001**, *45*, 5–32.
- (62) Chang, C.-C.; Lin, C.-J. LIBSVM: A Library for Support Vector Machines. *ACM Trans. Intell. Syst. Technol.* **2011**, *2*, 1.
- (63) Cortes, C.; Mohri, M.; Rostamizadeh, A. *Learning Non-linear Combinations of Kernels*, 2009; pp 396–404.
- (64) LeCun, Y.; Bengio, Y.; Hinton, G. Deep learning. *Nature* **2015**, *521*, 436–444.
- (65) Ke, G.; Meng, Q.; Finley, T.; Wang, T.; Chen, W.; Ma, W.; Ye, Q.; Liu, T.-Y. LightGBM: A Highly Efficient Gradient Boosting Decision Tree. *Adv. Neural Inf. Process. Syst.* **2017**, *30*, 3146–3154.
- (66) Friedman, J. H. Greedy function approximation: a gradient boosting machine. *Ann. Stat.* **2001**, *29*, 1189–1232.
- (67) Bajusz, D.; Rácz, A.; Héberger, K. 3.14-Chemical Data Formats, Fingerprints, and Other Molecular Descriptions for Database Analysis and Searching. In *Comprehensive Medicinal Chemistry III*, Chackalannil, S.; Rotella, D.; Ward, S. E., Eds.; Elsevier: Oxford, 2017; pp 329–378.
- (68) Sandfort, F.; Strieth-Kalthoff, F.; Kühnemund, M.; Beecks, C.; Glorius, F. A Structure-Based Platform for Predicting Chemical Reactivity. *Chem* **2020**, *6*, 1379–1390.
- (69) Sun, W.; Li, S.; Hu, R.; Qian, Y.; Wang, S.; Yang, G. Understanding solvent effects on luminescent properties of a triple

fluorescent ESIPT compound and application for white light emission. *J. Phys. Chem. A* **2009**, *113*, 5888–5895.

(70) Li, G.; Hirano, T.; Yamada, K. Bright near-infrared chemiluminescent dyes: Phthalhydrazides conjugated with fluorescent BODIPYs. *Dyes Pigm.* **2020**, *178*, 108339.

(71) Liu, J.; Zhu, L.; Wan, W.; Huang, X. Gold-Catalyzed Oxidative Cascade Cyclization of 1,3-Dynamides: Polycyclic N-Heterocycle Synthesis via Construction of a Europyridinyl Core. *Org. Lett.* **2020**, *22*, 3279–3285.

(72) Pei, K.; Zhou, H.; Yin, Y.; Zhang, G.; Pan, W.; Zhang, Q.; Guo, H. Highly fluorescence emissive 5, 5'-distyryl-3, 3'-bithiophenes: Synthesis, crystal structure, optoelectronic and thermal properties. *Dyes Pigm.* **2020**, *179*, 108396.

(73) Schüller, A.; Goh, G. B.; Kim, H.; Lee, J.-S.; Chang, Y.-T. Quantitative Structure-Fluorescence Property Relationship Analysis of a Large BODIPY Library. *Mol. Inf.* **2010**, *29*, 717–729.

(74) Chen, C.-H.; Tanaka, K.; Funatsu, K. Random forest approach to QSPR study of fluorescence properties combining quantum chemical descriptors and solvent conditions. *J. Fluoresc.* **2018**, *28*, 695–706.

(75) Bernini, C.; Zani, L.; Calamante, M.; Reginato, G.; Mordini, A.; Taddei, M.; Basosi, R.; Sinicropi, A. Excited State Geometries and Vertical Emission Energies of Solvated Dyes for DSSC: A PCM/TD-DFT Benchmark Study. *J. Chem. Theory Comput.* **2014**, *10*, 3925–3933.

(76) Savarese, M.; Aliberti, A.; De Santo, I.; Battista, E.; Causa, F.; Netti, P. A.; Rega, N. Fluorescence Lifetimes and Quantum Yields of Rhodamine Derivatives: New Insights from Theory and Experiment. *J. Phys. Chem. A* **2012**, *116*, 7491–7497.

(77) Brown, A.; Ngai, T. Y.; Barnes, M. A.; Key, J. A.; Cairo, C. W. Substituted Benzoxadiazoles as Fluorogenic Probes: A Computational Study of Absorption and Fluorescence. *J. Phys. Chem. A* **2012**, *116*, 46–54.

(78) Jacquemin, D.; Perpète, E. A.; Scalmani, G.; Frisch, M. J.; Assfeld, X.; Ciofini, I.; Adamo, C. Time-dependent density functional theory investigation of the absorption, fluorescence, and phosphorescence spectra of solvated coumarins. *J. Chem. Phys.* **2006**, *125*, 164324.

(79) Jacquemin, D.; Perpète, E. A.; Scalmani, G.; Ciofini, I.; Peltier, C.; Adamo, C. Absorption and emission spectra of 1,8-naphthalimide fluorophores: A PCM-TD-DFT investigation. *Chem. Phys.* **2010**, *372*, 61–66.

(80) Grimme, S.; Neese, F. Double-hybrid density functional theory for excited electronic states of molecules. *J. Chem. Phys.* **2007**, *127*, 154116.

(81) Fabrizio, A.; Meyer, B.; Corminboeuf, C. Machine learning models of the energy curvature vs particle number for optimal tuning of long-range corrected functionals. *J. Chem. Phys.* **2020**, *152*, 154103.

(82) Qiao, Z.; Welborn, M.; Anandkumar, A.; Manby, F. R.; Miller, T. F., III OrbNet: Deep learning for quantum chemistry using symmetry-adapted atomic-orbital features. *J. Chem. Phys.* **2020**, *153*, 124111.

(83) Westermayr, J.; Marquetand, P. Machine Learning for Electronically Excited States of Molecules. *Chem. Rev.* **2020**, DOI: [10.1021/acs.chemrev.0c00749](https://doi.org/10.1021/acs.chemrev.0c00749).

(84) Ju, C.-W.; Liu, R.; Bai, H.; Li, B. *ChemFluor. Figshare* 2020.report